Recycling Used-Coffee Grounds into Hierarchical Nanostructured Carbon for Supercapacitor Application

Article *in* Asian Journal of Chemistry · July 2023

DOI: 10.14233/ajchem.2023.28035

5 authors, including:

Roselin Ranjitha Mathiarasu
Bridge Green Upcycle Pvt Ltd
12 PUBLICATIONS **179** CITATIONS
SEE PROFILE

Thileep Kumar Kumaresan
Korea Institute of Energy Technology
23 PUBLICATIONS **333** CITATIONS
SEE PROFILE

Raghu Sangeetha
Oregon State University
77 PUBLICATIONS **2,261** CITATIONS
SEE PROFILE

Asian Journal of Chemistry; Vol. 35, No. 7 (2023), 1749-1755

ASIAN JOURNAL OF CHEMISTRY

https://doi.org/10.14233/ajchem.2023.28035

Recycling Used-Coffee Grounds into Hierarchical Nanostructured Carbon for Supercapacitor Application

C. RAJASEKAR[1], M. ROSELIN RANJITHA[2], K. THILEEP KUMAR[3], RA. KALAIVANI[1,*] and S. RAGHU[4,*]

[1]Department of Chemistry, Vels Institute of Science, Technology & Advanced Studies (VISTAS), Chennai-600117, India
[2]Department of Chemistry, Stella Maris College (Autonomous) (affiliated to University of Madras), Chennai-600086, India
[3]Advanced Energy Material Laboratory, Department of Advanced Components and Material Engineering, Sunchon National University, Suncheon, Jeollanam-do, 579-22, Republic of Korea
[4]Centre for Advanced Research and Development (CARD)/Chemistry, Vels Institute of Science, Technology & Advanced Studies (VISTAS), Chennai-600117, India

*Corresponding authors: E-mail: rakvani@yahoo.co.in; subraghu_0612@yahoo.co.in

Received: 16 May 2023; *Accepted*: 15 June 2023; *Published online*: 6 July 2023; AJC-21302

Hierarchical nanostructured activated carbon electrode material was prepared from the used-coffee grounds to fabricate a cost-effective, scalable and high-performance symmetric supercapacitor. The interconnected, disordered and microporous material was synthesized in a simple two-stage method of chemical activation with zinc chloride followed by direct pyrolysis of the coffee grounds at 900 ºC in nitrogen atmosphere. The N_2 adsorption and desorption analysis showed that the prepared material had an extraordinary surface area of ~1178 $m^2 g^{-1}$. The fabricated symmetric supercapacitor device in non-aqueous tetraethylammonium tetrafluoroborate ($TEABF_4$) electrolyte exhibited 2.7 V cell voltage with superior specific capacitance, energy and power density of 129 F g^{-1}, 56.4 Wh kg^{-1} and 797.9 W kg^{-1}, respectively. Besides, it also had a high specific capacitance retention of 99% even after 10,000 cycles. This work demonstrated an effective approach to transform coffee grounds into high performance electrode material for renewable energy devices. The observed electrochemical performance evidently showed that the materials derived from waste coffee grounds could be recycled into potential electrode material for supercapacitors. The cost-effectiveness and abundance of waste coffee grounds combined with the simple activation process and high performance of the synthesized material increased its feasibility for commercial applications in energy storage devices.

Keywords: Nanostructured carbon, Symmetric supercapacitors, Used-coffee grounds, Non-aqueous electrolyte.

INTRODUCTION

The world is facing a constant rising demand for sustainable and renewable energy sources [1-3]. Supercapacitors, an established electrochemical energy storage system with enhanced charge/discharge rate, cycle life and power density have emerged as a promising solution to overcome this challenging situation. However, developing an efficient less-expensive super-capacitor electrode material remains a critical issue [4,5]. In this context, recycling waste materials into potential sources of renewable low-cost electrode materials has gained significant attention. One such material is used coffee grounds, which is generated in large quantities worldwide and typically discarded as waste [6-9]. Notably, coffee is one of the most significant commercial crops and is cultivated over 11 million hectares worldwide.

Next to petroleum-related commodities, coffee marks the second most-traded and consumed product globally. Owed to its high consumption and trade, coffee industry generates a considerable amount of byproducts and waste which eventually leads to environmental pollution [10-12]. Recent studies have shown that used-coffee grounds (UCG) can be converted into hierarchical nanostructured activated carbon (HNAC) material, which exhibits excellent electrochemical properties and can be incorporated as an electrode material in supercapacitors [13-15]. A previous reports have proposed the synthesis strategy to convert UCG into activated carbon and integrated it into an aqueous electric double layer capacitor (EDLC), which could operate up to 1.2 V [16,17]. When compared with aqueous electrolytes, elevated energy densities can be achieved with organic electrolytes since the cell voltage can be increased

upto 2.7 V. This is attributed to the restricted transport of bulky organic-salt ions within the narrow carbon pores during fast charge-discharge rates, unlikely with the H_2SO_4 or KOH ions [18-20]. This study presents an innovative two-stage preparation process to recycle UCG into a high-performance supercapacitor electrode material.

EXPERIMENTAL

The used-coffee grounds (UCG) were obtained from a local filter-coffee shop and also from different residential areas of Chennai, India. $ZnCl_2$, Teflon solution (60%) and conducting carbon (super P) were purchased from Sigma-Aldrich. The analytical grade chemicals were used throughout the experiments without any further purification.

Preparation of hierarchical nanostructured activated carbon (HNAC) from used-coffee grounds (UCG): High temperature chemical activation method was employed for the synthesis of HNAC derived from UCG. The obtained carbon was then treated with a pore-forming substance ($ZnCl_2$) at a peel:porogen weight ratio of 1:3. This mixture was mixed homogenously and soaked for 6 h followed by which it was dried at 120 ºC in vacuum air oven for 6 h. Preparation of activated carbon was carried out in a tubular furnace at 800 and 900 ºC for 2 h under N_2 gas with a heating rate 5 ºC/min. The obtained activated carbon materials were washed thoroughly with 3 M HCl and de-ionized water to remove unwanted residues. Finally, they were dried at 100 ºC in vacuum air oven for 12 h. The synthesized HNACs were denoted by their annealing temperatures (HNAC-800 & HNAC-900) and were utilized as electrode materials for the fabrication of supercapacitors.

Preparation of electrode film and electrochemical measurements: To evaluate the electrochemical properties of as-synthesized HNACs electrodes were fabricated by mixing with 85% active material, 10% conducting carbon, 5% Teflon solution and isopropyl alcohol (IPA) as solvent. This mixture was continuously mixed until it formed a homogenous paste which was then made into a film. Further, the film was dried at 100 ºC in vacuum oven. Electrodes for the supercapacitor cells were fabricated to assess the capacitive properties of the HNACs. The symmetric devices constructed with CR2032 coin cells had two electrodes separated by microfiber glass-filter papers with ~0.18 µm thickness. Specific capacitance (C), energy density (E) and power density (P) were calculated using the following equations (eqns. 1-3), respectively [21].

$$C = \frac{4I \times \Delta t}{m \times \Delta V} \quad (1)$$

$$E = \frac{½CV^2}{8} \quad (2)$$

$$P = \frac{E \times 3600}{t} \quad (3)$$

where C = specific capacitance (F g^{-1}); I = applied current density, t = discharge time, m = total mass of both electrodes and ΔV = voltage drop of discharging curve, E = specific energy (Wh kg^{-1}), V = potential (Volts) and P = specific power (W kg^{-1}).

Electrochemical analysis: To evaluate the potential electrochemical performance of HNACs derived from UGC, they were compared with both aqueous and non-aqueous electrolytes. The electrochemical measurements were performed in a SP-300 Biologic EC lab workstation and Neware battery setup using a symmetrical two electrode configuration with 6 M KOH (aqueous) and tetraethylammonium tetrafluoroborate ($TEABF_4$, non-aqueous) as electrolyte.

RESULTS AND DISCUSSION

The schematic representation for the conversion of UCG into HNACs is represented in Fig. 1. Since, it is evident that UCG consists high volumes of organic carbon and caffeine, it is expected to form nanostructured activated carbon materials with nanoporosity and higher surface area depending on the gas flow rate at higher temperatures.

XRD studies: The XRD spectrum of the prepared HNACs are depicted in Fig. 2a. In HNAC-800, the (002) and (101) planes of carbon appeared at 30.8º and 42.2º. This showed that HNAC-800 has both crystalline and amorphous nature with $d_{(002)}$ interlayer spacing 4.12 Å, which is due to the π-π stacked layers. However, HNAC-900 showed (002) and (101) planes at 24.5º and 41.5º with $d_{(002)}$ interlayer spacing (3.55 Å). Notably, the peak intensity of HNAC-900 was greater than that of HNAC-800. It is also evidenced that HNAC-800 had amorphous nature and it does not contain any graphitic peak. But when the activation temperature was increased to 900 ºC (HNAC-900), the sample was amorphous and had graphitic peak [22]. Thus it is clear that the graphitic peaks of HNAC-900 are due to the presence of 99% sp^2 hybridized carbon bonding. The Scherrer's equation was used to assess the number of stacked graphene layers and is depicted in Table-1. Remarkably, this work is the first-ever reported synthesis of UCG-derived HNAC to obtain high degrees of graphitic nature at lower temperature (900 ºC).

Raman studies: Structure and quality of the HNACs were analyzed by Raman spectroscopy (Fig. 2b). The obtained results confirmed the parameters such as defects, disorder (D bands)

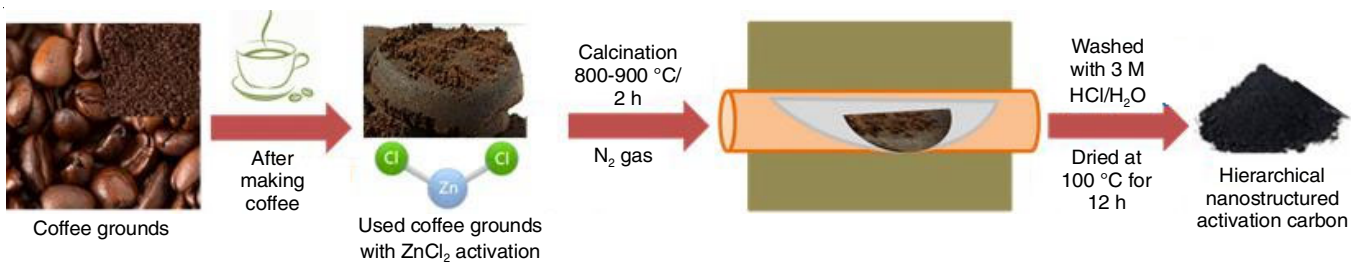

Fig. 1. Schematic representation for the conversion of used-coffee grounds (UCG) into hierarchical nanostructured activated carbon (HNAC)

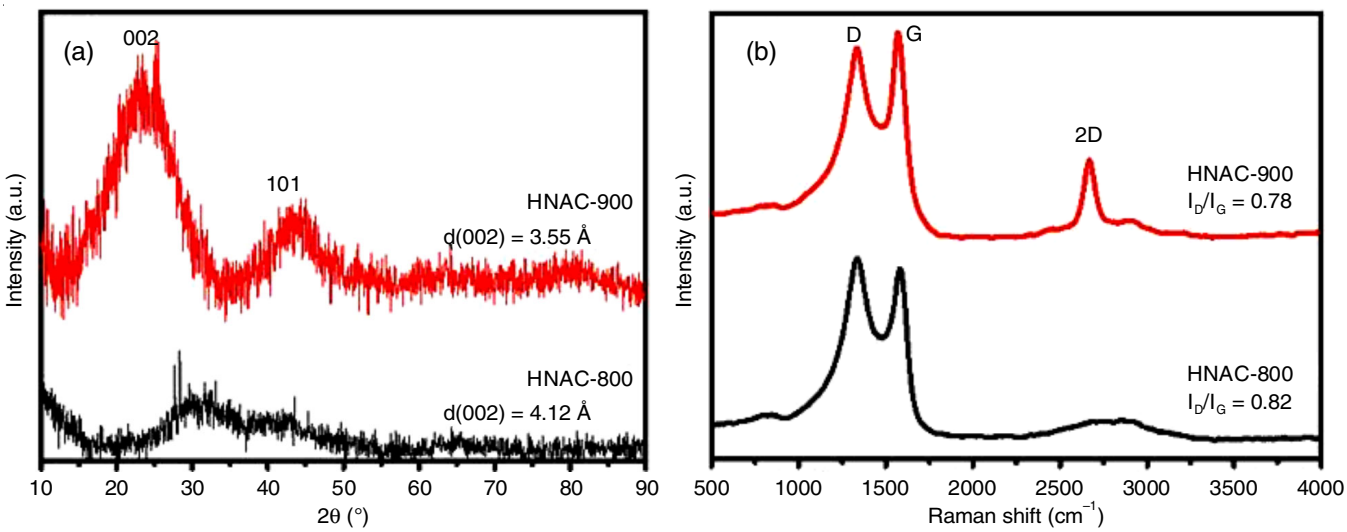

Fig. 2. (a) XRD pattern and (b) Raman spectra of HNACs materials thermally treated for HNAC-800 and HNAC-900

TABLE-1
XRD PARAMETERS OF DIFFERENT CARBON SAMPLES

Samples	002 peak (°)	$d_{(002)}$ (Å)	FWHM	L_a (nm)
HNAC-800	30.8	4.12	26.9	0.52
HNAC-900	24.5	3.55	20.8	0.58

and graphitic nature (G bands). In general, the G band mirrors the imperfections in the graphitic sp^2 carbon structure by reflecting the structural defects/partially disordered graphitic domains [23]. The HNAC-800 exhibited two distinctive peaks at 1332 and 1580 cm^{-1}, which corresponded to the D and G bands. In addition, a broad peak attributed to the 2D band appeared at 2668 cm^{-1}. The HNAC-900 sample presented three fundamental peaks at 1337.8 cm^{-1} (D band), 1580.5 cm^{-1} (G band) and 2671 cm^{-1} (2D band). From the Raman spectrum, the high intensity peak for 2D band appeared only for HNAC-900 at 2671 cm^{-1}.

The crystallite size (L_a) was calculated using the equation: $L_a = I_G/I_D \times C\lambda$ [24]. The degree of disorderliness in the structure of carbon-based materials can be determined using the I_D/I_G value. Additionally, this value is proportionate to the crystal nature of the material whereas the stacking and number of graphene layers can be found using I_{2D}/I_G value. The obtained results showed that the I_D/I_G value is inversely proportional to the activation temperature *i.e.* as the activation temperature of carbon increases, the I_D/I_G value decreases. As validated by XRD analysis, Raman studies of also re-confirmed the presence of highly-ordered graphitic planes made up of irregular polycyclic hydrocarbons. These planes were surrounded by amorphous carbon clusters, which resulted from the pyrolysis of non-aromatic side chains.

BET studies: The BET isotherms and pore size distribution of the prepared UCG-derived HNACs are as displayed in Fig. 3. The isotherms plots of both the HNACs followed Type-I isotherm [25]. Surface area of HNAC-800 and HNAC-900 was found to be 1052 and 1178 $m^2\ g^{-1}$, respectively. The HNAC material activated at 900 ºC exhibited a larger surface area and is tabulated in Table-2. Thereby, HNAC-900 is expected to have enhanced electrochemical properties in comparison with HNAC-800. This superior surface area of HNAC-900 provides various paths of diffusion and transporting ions, which could penetrate through

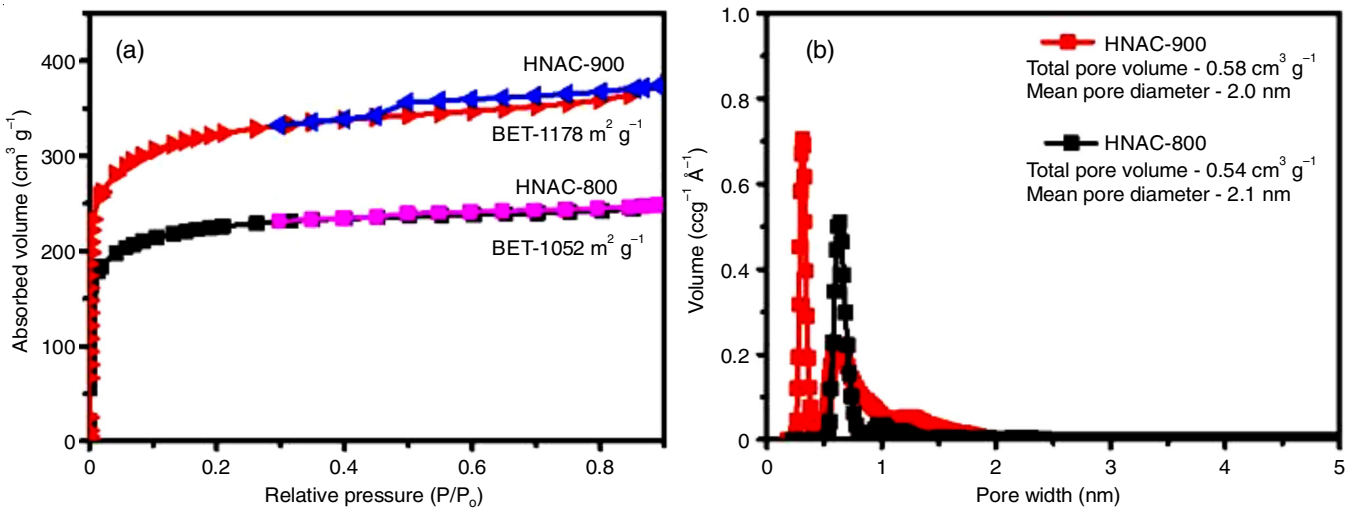

Fig. 3. (a) N_2 adsorption isotherms of the HNACs materials and (b) power spectral densities (PSD) comparison of HNACs materials

TABLE-2
RAMAN SPECTRUM I_D/I_G VALUES AND BET SURFACE VALUES OF DIFFERENT CARBON SAMPLES

Samples	I_D/I_G	BET surface area ($m^2 g^{-1}$)	Mean pore diameter (nm)	Total pore volume ($cm^3 g^{-1}$)
HNAC-800	0.82	1052	2.1	0.54
HNAC-900	0.78	1178	2.0	0.58

the electrolyte. Additionally, it contributes to the increased active sites for feasible electrode-electrolyte reactions. Adsorption enhanced at low relative pressures leading to the formation of highly micro-porous materials with narrow pore size distribution. Particularly, the hysteresis witnessed for pore width lesser than 4 nm corresponded to the mesopores of the material. HNAC-900 sample exihibits a high synergic effect through which it safeguards the electrode material in charge-discharge process. It also creates an interconnected pathways to facilitate the transportation of electrolyte and accelerate the diffusion of electrons. Based on the obtained data, surface area of the HNACs is expected to have a significant relationship with the electrochemical properties. The HNAC-900 sample with the superior surface area could demonstrate good characteristics in capacitance, energy and power of the supercapacitor cell.

FTIR studies: FTIR spectrum of HNACs are depicted in Fig. 4a. The prepared HNAC-800 had five distinct peaks at 2956.8, 2262.5, 1980.2, 1576.5 and 1157.8 cm^{-1}, which correlated with the vibrations of C-H, C≡C, C=O, C=C and C-C stretching, respectively. In comparison, HNAC-900 had four distinct peaks at 2938.5, 2278.2, 1525.6 and 1087.8 cm^{-1} which corresponded to the vibrations of C-H, C≡C, C-H bending and C-C stretching, respectively. The spectrum showed a decreasing trend in the number of peaks. On increasing the activation temperature from 800 to 900 ºC, the carbon-carbon bond increased with the simultaneous removal of functional groups [26]. Thus, the activation temperature and functional groups of the HNACs were found to be inversely proportional.

HRSEM analysis: The morphology and surface texture of the UCG-derived HNACs were explored using HRSEM technique. HRSEM image of the untreated-UCG is showed in Fig. 4b as well as the images of HNACs that were pyrolyzed at 800 ºC and 900 ºC are presented in Fig. 4c,d. The untreated-UCG was completely clumped together and had uneven morphology. However, after being activated with $ZnCl_2$ and exposed to high temperatures (900 ºC) it became porous and flaky. When compared with untreated-UGC and HNAC-800, it is clearly seen that HNAC-900 sample has enhanced surface porosity, which showed its superior surface area.

Electrochemical studies: To substantiate the electrochemical performance of HNACs, they were incorporated as electrode materials in the symmetric supercapacitors (SSCs).

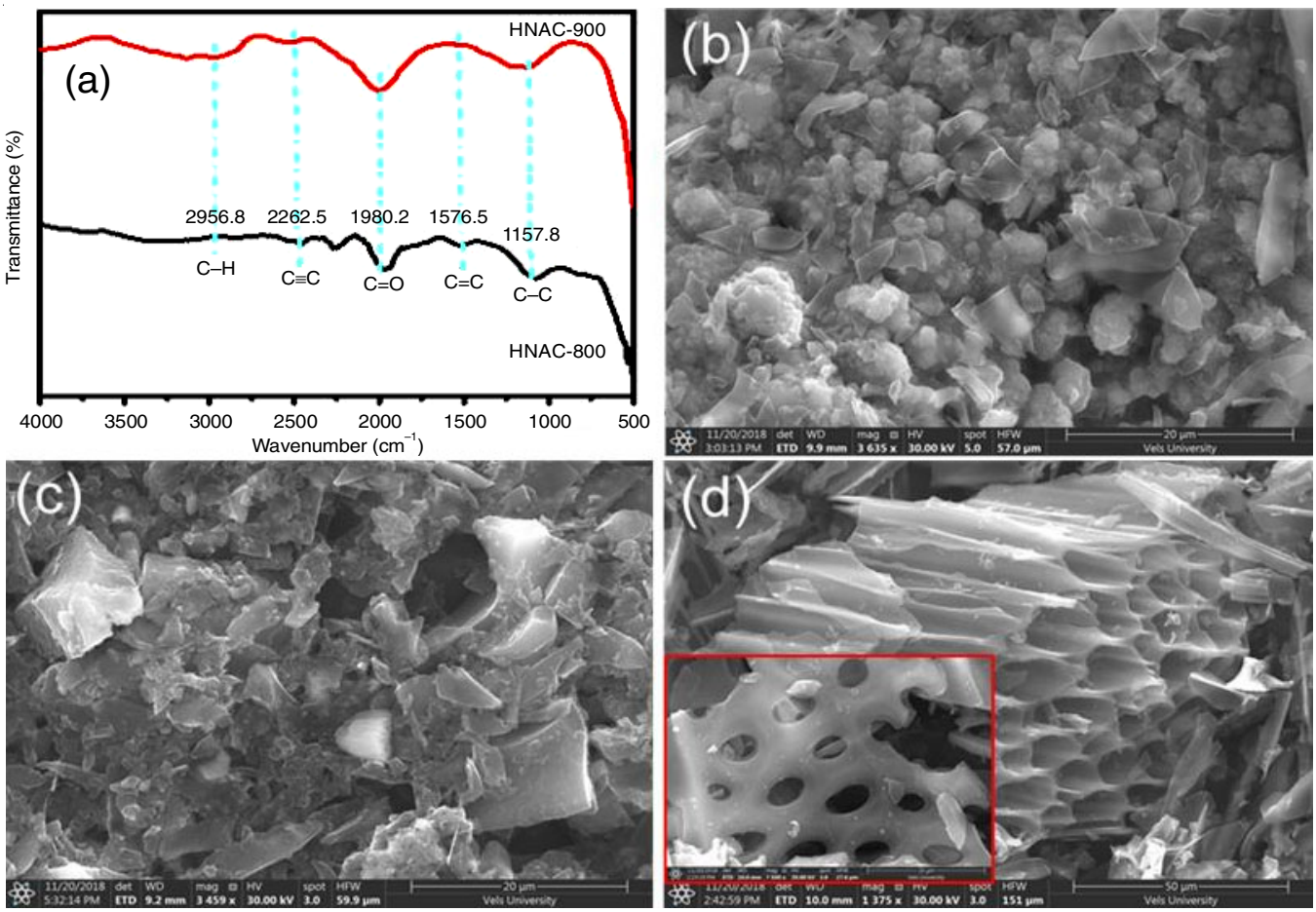

Fig. 4. (a) FTIR spectrum of prepared HNACs and (b) The HRSEM images of untreated-UGC, (c) HNAC-800 (d) HNAC-900 (Inset: SEM image at 10 μm magnification)

The cyclic voltammetry (CV) study was carried out with HNAC-800 and HNAC-900 samples as the electrodes and is represented in Fig. 5a,b. The voltage ranges of 0-1.2 V and 0-2.7 V was used for the aqueous (KOH) and non-aqueous ($TEABF_4$) electrolytes. All the CV curves were almost rectangular in shape and they exhibited a good symmetry [27]. Further, galvanostatic charge-discharge (GCD) analysis was performed at the same potential window used for the CV experiment. The GCD profiles of both HNACs with aqueous and non-aqueous electrolytes at different current densities are depicted in Fig. 6a-d. The cycling stability of symmetric supercapacitors with HNACs using both aqueous and non-aqueous electrolytes was assessed by conducting GCD measurements for 10,000 cycles at a current density of 1 A g^{-1} (Fig. 6e). Notably, HNAC-900 with 6 M aqueous electrolyte (KOH) and non-aqueous ($TEABF_4$) electrolytes demonstrated exceptional cyclic stability and retained approximately 95% of their capacitance. The HNAC-900 sample represented the superior specific capacitance 129 F g^{-1}, energy density 56.4 Wh kg^{-1} and powder density 797.9 W kg^{-1} (Table-3). Based on the obtained data, it is proved that the surface area

TABLE-3
SPECIFIC CAPACITANCE, ENERGY DENSITY AND POWER DENSITY OF THE HNACs

Samples	Electrolyte	Specific capacitance (F g^{-1})	Energy density (Wh kg^{-1})	Power density (W kg^{-1})
HNAC-800	KOH	228	20.52	295.5
	$TEABF_4$	112	47.6	774.0
HNAC-900	KOH	295	26.55	324
	$TEABF_4$	129	56.4	797.9

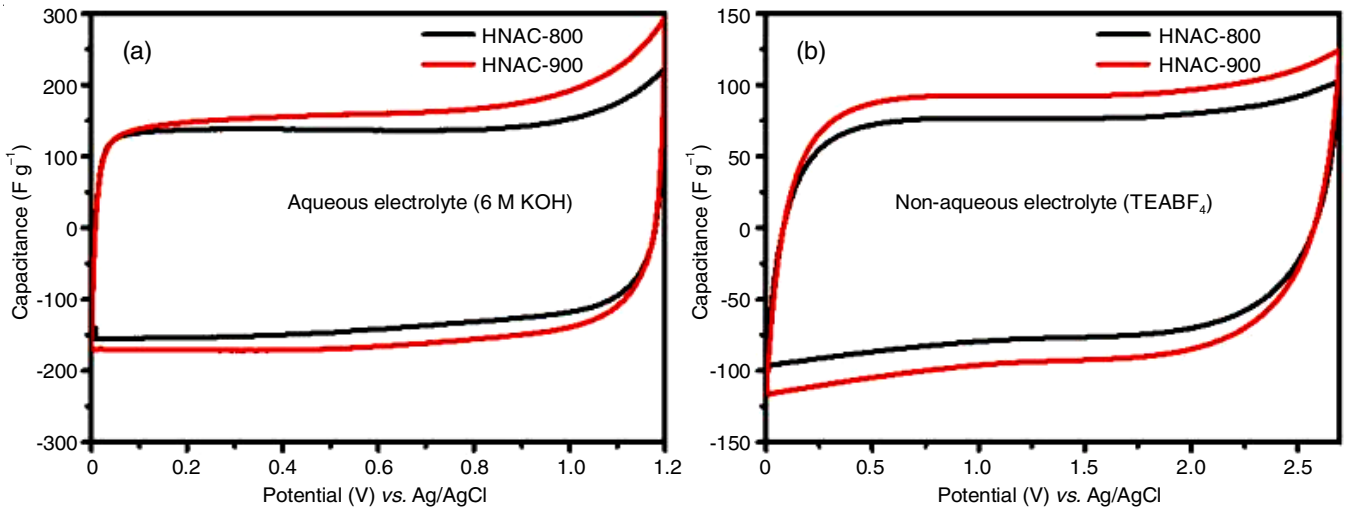

Fig. 5. Cyclic voltammetry of as-prepared carbons (a) aqueous electrolyte and (b) non-aqueous electrolyte

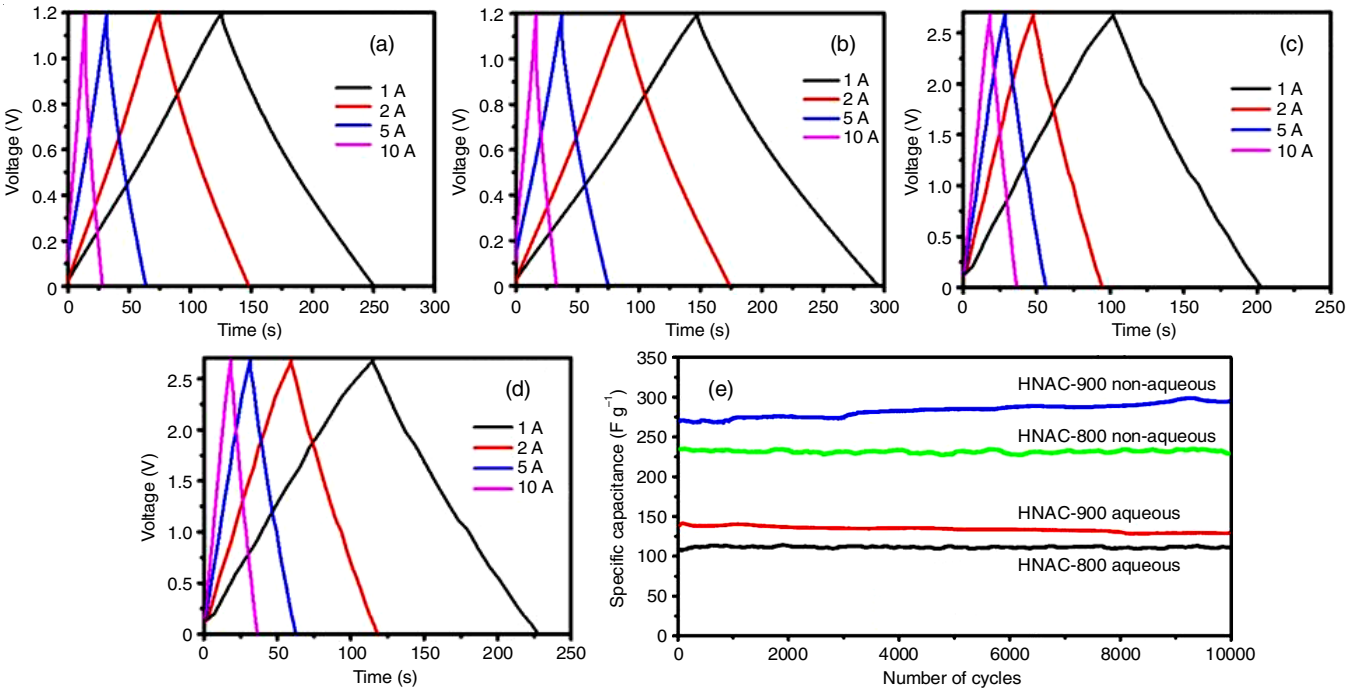

Fig. 6. Galvanostatic charge-discharge curve of prepared HNACs (a) HNAC-800-aqueous, (b) HNAC-900-aqueous, (c) HNAC-800-non-aqueous, (d) HNAC-900-non-aqueous and (e) Long-term cycling study of the prepared HNACs

TABLE-4
COMPARATIVE STUDY WITH OTHER WASTE-DERIVED SUPERCAPACITORS

Waste material	Activation method	Electrolyte	Specific capacitance (F g^{-1})	Capacitance retention	Cycling stability (%)	Ref.
Banana fiber	10% $ZnCl_2$	1 M Na_2SO_4	74 F g^{-1} @ 0.5 A g^{-1}	500	87.83	[28]
Coconut shell	Steam 3000	6 M KOH	~100 F g^{-1} @ 1 A g^{-1}	3000	61.29	[29]
Coffee bean	(1:2 ratio) H_3PO_4	1 M H_2SO_4	33–35 F g^{-1} @ 1A g^{-1}	10,000	~ 82	[30]
Jute fiber	(1:1 ratio) KOH	3 M KOH	51 F g^{-1} @ 1 mV s^{-1}	5000	100	[31]
Tyre	(1:9 ratio) H_3PO_4	6 M KOH	49 F g^{-1} @ 1 A g^{-1}	1000	97	[32]
HNAC-900	(1:3 ratio) $ZnCl_2$	$TEABF_4$	129 F g^{-1} @ 1 A g^{-1}	10,000	100	Present work

of the HNACs have a significant relationship with its electrochemical properties. However when compared with the reported literature in Table-4, HNAC-900 has a higher surface area and accordingly it demonstrated superior capacitance, energy and power in the supercapacitor cell.

Conclusion

This work highlights the potential use of used-coffee grounds (UGC) as waste in supercapacitors as a low-cost and renewable source of electrode material. Two samples HNAC-800 and HNAC-900 were synthesized based on varying annealing temperatures (800 and 900 ºC). Remarkably, the SSC fabricated with HNAC-900 and $TEABF_4$ electrolyte exhibited a superior specific capacitance 129 F g^{-1}, energy density 56.4 Wh kg^{-1} and power density 797.9 W kg^{-1} with excellent cycling stability. High performance, scalability and simplicity of activation technique indicate its potential for commercial applications in super-capacitors. This approach not only provides a second life to waste-UGC but also addresses the growing need for sustainable and ecofriendly solutions in energy storage field.

CONFLICT OF INTEREST

The authors declare that there is no conflict of interests regarding the publication of this article.

REFERENCES

1. B. Dyatkin, V. Presser, M. Heon, M.R. Lukatskaya, M. Beidaghi and Y. Gogotsi, *ChemSusChem*, **6**, 2269 (2013); https://doi.org/10.1002/cssc.201300852
2. K. Thileep Kumar, G. Sivagaami Sundari, E. Senthil Kumar, A. Ashwini, M. Ramya, P. Varsha, R. Kalaivani, M. Shanmugaraj Andikkadu, V. Kumaran, R. Gnanamuthu, S.Z. Karazhanov and S. Raghu, *Mater. Lett.*, **218**, 181 (2018); https://doi.org/10.1016/j.matlet.2018.02.017
3. L. Wan, J. Wang, L. Xie, Y. Sun and K. Li, *ACS Appl. Mater. Interfaces*, **6**, 15583 (2014); https://doi.org/10.1021/am504564q
4. A.G. Pandolfo and A.F. Hollenkamp, *J. Power Sources*, **157**, 11 (2006); https://doi.org/10.1016/j.jpowsour.2006.02.065
5. J. Tang, R.R. Salunkhe, J. Liu, N.L. Torad, M. Imura, S. Furukawa and Y. Yamauchi, *J. Am. Chem. Soc.*, **137**, 1572 (2015); https://doi.org/10.1021/ja511539a
6. Y.J. Hwang, S.K. Jeong, K.S. Nahm, J.S. Shin and A. Manuel Stephan, *J. Phys. Chem. Solids*, **68**, 182 (2007); https://doi.org/10.1016/j.jpcs.2006.10.007
7. C. Kourmentza, Ch.N. Economou, P. Tsafrakidou and M. Kornaros, *J. Clean. Prod.*, **172**, 980 (2018); https://doi.org/10.1016/j.jclepro.2017.10.088
8. J.M.V. Nabais, P. Nunes, P.J.M. Carrott, M.M.L. Ribeiro Carrott, A.M. García and M.A. Díaz-Díez, *Fuel Process. Technol.*, **89**, 262 (2008); https://doi.org/10.1016/j.fuproc.2007.11.030
9. V. Boonamnuayvitaya, S. Sae-Ung and W. Tanthapanichakoon, *Sep. Purif. Technol.*, **42**, 159 (2005); https://doi.org/10.1016/j.seppur.2004.07.007
10. J.-H. Bae, J.-H. Park, S.-S. Im and D.-K. Song, *Intergr. Med. Res.*, **3**, 189 (2014); https://doi.org/10.1016/j.imr.2014.08.002
11. T. Tian, S. Freeman, M. Corey, J.B. German and D. Barile, *J. Agric. Food Chem.*, **65**, 2784 (2017); https://doi.org/10.1021/acs.jafc.6b04716
12. R.C. Alves, I.M.C. Almeida, S. Casal and M.B.P.P. Oliveira, *J. Agric. Food Chem.*, **58**, 3002 (2010); https://doi.org/10.1021/jf9039205
13. Y.S. Yun, M.H. Park, S.J. Hong, M.E. Lee, Y.W. Park and H.J. Jin, *ACS Appl. Mater. Interfaces*, **7**, 3684 (2015); https://doi.org/10.1021/am5081919
14. M. Biegun, A. Dymerska, X. Chen and E. Mijowska, *Materials*, **13**, 3919 (2020); https://doi.org/10.3390/ma13183919
15. J. Choi, C. Zequine, S. Bhoyate, W. Lin, X. Li, P. Kahol and R. Gupta, *J. Carbon Res.*, **5**, 44 (2019); https://doi.org/10.3390/c5030044
16. T.E. Rufford, D. Hulicova-Jurcakova, Z. Zhu and G.Q. Lu, *Electrochem. Commun.*, **10**, 1594 (2008); https://doi.org/10.1016/j.elecom.2008.08.022
17. N.L. Torad, R.R. Salunkhe, Y. Li, H. Hamoudi, M. Imura, Y. Sakka, C.C. Hu and Y. Yamauchi, *Chem. Eur. J.*, **20**, 7895 (2014); https://doi.org/10.1002/chem.201400089
18. Y.-J. Kim, Y. Masutzawa, S. Ozaki, M. Endo and M.S. Dresselhaus, *J. Electrochem. Soc.*, **151**, E199 (2004); https://doi.org/10.1149/1.1715095
19. Y.H. Chiu and L.Y. Lin, *J. Taiwan Inst. Chem. Eng.*, **101**, 177 (2019); https://doi.org/10.1016/j.jtice.2019.04.050
20. M. Endo, T. Maeda, T. Takeda, Y.J. Kim, K. Koshiba, H. Hara and M.S. Dresselhaus, *J. Electrochem. Soc.*, **148**, A910 (2001); https://doi.org/10.1149/1.1382589
21. Z. Pan, Z. Lu, L. Xu and D. Wang, *Appl. Surf. Sci.*, **510**, 145384 (2020); https://doi.org/10.1016/j.apsusc.2020.145384
22. E. Kusrini, F. Oktavianto, A. Usman, D.P. Mawarni and M.I. Alhamid, *Appl. Surf. Sci.*, **506**, 145005 (2020); https://doi.org/10.1016/j.apsusc.2019.145005
23. F.E.C. Othman, N. Yusof, S. Samitsu, N. Abdullah, M.F. Hamid, K. Nagai, M.N.Z. Abidin, M.A. Azali, A.F. Ismail, J. Jaafar, F. Aziz, W.N.W. Salleh, *J. CO2 Util.*, **45**, 101434 (2021); https://doi.org/10.1016/j.jcou.2021.101434
24. A. Ghosh, C.A. Razzino, A. Dasgupta, K. Fujisawa, L.H.S. Vieira, S. Subramanian, R.S. Costa, A.O. Lobo, O.P. Ferreira, J. Robinson, M. Terrones, H. Terrones and B.C. Viana, *Carbon*, **145**, 175 (2019); https://doi.org/10.1016/j.carbon.2018.12.114
25. E. Elaiyappillai, R. Srinivasan, Y. Johnbosco, P. Devakumar, K. Murugesan, K. Kesavan and P.M. Johnson, *Appl. Surf. Sci.*, **486**, 527 (2019); https://doi.org/10.1016/j.apsusc.2019.05.004

26. E. Yagmur, Y. Gokce, S. Tekin, N.I. Semerci and Z. Aktas, *Fuel*, **267**, 117232 (2020); https://doi.org/10.1016/j.fuel.2020.117232
27. Q. Wu, D. Liang, X. Ma, S. Lu and Y. Xiang, *RSC Adv.*, **9**, 26676 (2019); https://doi.org/10.1039/C9RA04959B
28. V. Subramanian, C. Luo, A.M. Stephan, K.S. Nahm, S. Thomas and B. Wei, *J. Phys. Chem. C*, **111**, 7527 (2007); https://doi.org/10.1021/jp067009t
29. J. Mi, X.R. Wang, R.J. Fan, W.H. Qu and W.C. Li, *Energy Fuels*, **26**, 5321 (2012); https://doi.org/10.1021/ef3009234
30. C. Huang, T. Sun and D. Hulicova-Jurcakova, *ChemSusChem*, **6**, 2330 (2013); https://doi.org/10.1002/cssc.201300457
31. C. Zequine, C.K. Ranaweera, Z. Wang, P.R. Dvornic, P.K. Kahol, S. Singh, P. Tripathi, O.N. Srivastava, S. Singh, B.K. Gupta, G. Gupta and R.K. Gupta, *Sci. Rep.*, **7**, 1174 (2017); https://doi.org/10.1038/s41598-017-01319-w
32. M. Zhi, F. Yang, F. Meng, M. Li, A. Manivannan and N. Wu, *ACS Sustain. Chem. Eng.*, **2**, 1592 (2014); https://doi.org/10.1021/sc500336h